# High-field magnetization of $Ho_2Fe_{17}$

Y. Skourski,[1,*] M. D. Kuz'min,[2] K. P. Skokov,[2,3] A. V. Andreev,[4] and J. Wosnitza[1]

[1]*Dresden High Magnetic Field Laboratory, Helmholtz-Zentrum Dresden Rossendorf, D-01314 Dresden, Germany*

[2]*Leibniz-Institut für Festkörper- und Werkstoffforschung, PF 270116, D-01171 Dresden, Germany*

[3]*Faculty of Physics, Tver State University, 33 Gelabova Street, Tver 170002, Russia*

[4]*Institute of Physics ASCR, Na Slovance 2, CZ-18221 Prague, Czech Republic*

(Received 24 February 2011; revised manuscript received 18 April 2011; published 15 June 2011)

The magnetization of a $Ho_2Fe_{17}$ single crystal has been measured along the principal crystallographic directions in pulsed magnetic fields up to 60 T. Stepwise discontinuities in the magnetization occur at 45 and 55 T along the [120] and [100] directions, respectively. The data allowed us to deduce the molecular field at the Ho site. As a cross check, the molecular field was determined as well from a magnetization measurement when the $Ho_2Fe_{17}$ single crystal was let rotate freely. Both values are in good agreement with each other.

DOI: 10.1103/PhysRevB.83.214420 PACS number(s): 75.30.Et, 75.30.Kz

## I. INTRODUCTION

Rare-earth-iron intermetallic compounds are important magnetic materials, valued for their high magnetic anisotropy.[1] It originates from the crystal field acting on the rare earth and is mediated by an exchange interaction coupling the rare earth and the iron sublattices with each other. The strength of this coupling, thus, appears to be an important characteristic of a hard magnetic material, perhaps even more important than the leading crystal-field parameter $A_{20}$.[2] Unambiguous experimental determination of the intersublattice exchange in strongly anisotropic magnets is difficult because it cannot be easily disentangled from the strong, *a priori* unknown crystal field. Ferrimagnetic compounds with heavy rare earths—less suitable for applications than their ferromagnetic light rare-earth counterparts, but then amenable to high-field experiments — present additional possibilities for circumventing the above difficulties. $Ho_2Fe_{17}$ is supposed to be a well-studied ferrimagnet. Starting from 1980, several single crystals were produced and measurements of magnon dispersion[3,4] and high-field magnetization[5,6] curves were carried out. Relevant model parameters were deduced independently from both data sets. Rather unexpectedly, one finds no consensus in the published results. For instance, the molecular field at the holmium site, $H_{\rm mol}$, determined from the neutron data equals 58.5 T,[4] whereas the high-field magnetization data yield a 1.5 times higher value,[5,6] 88 T (both values refer to $T = 4.2$ K). This discrepancy remained unexplained.

Strictly speaking, there are two nonequivalent Ho sites in the hexagonal $Th_2Ni_{17}$-type structure of $Ho_2Fe_{17}$ and, correspondingly, two different values of $H_{\rm mol}$. However, the difference appears insignificant, as can be judged by the $^{161}$Dy Mössbauer spectra of the isomorphous $Dy_2Fe_{17}$; these were successfully described by a single set of hyperfine parameters even at room temperature.[7] Therefore, the Ho atoms in $Ho_2Fe_{17}$ are usually regarded as equivalent.[3–6,8–10] Such an approximation will be adopted in this work, too.

For other model parameters of $Ho_2Fe_{17}$, one finds disparate reports. As an example, Table I presents a compilation of published values of the crystal-field parameter $A_6^6\langle r^6\rangle$ (converted to the same notation[11]) as well as of the basal-plane anisotropy constant of the Ho sublattice $K_4^{\rm Ho}$ at $T = 0$. The latter is connected with the former through a simple proportionality relation,[12]

$$K_4^{\rm Ho} = -\tfrac{50}{429} A_6^6\langle r^6\rangle. \quad (1)$$

Here, $K_4^{\rm Ho}$ is normalized per Ho atom. Note that the proportionality factor used by Clausen[3] was 2.9 times too high;[13] Table I presents the corrected result. Here, we refer solely to anisotropy constants for a two-sublattice model, where the Ho and Fe sublattices are not rigidly antiparallel. The neglect of such noncollinearity led to contradictory results in earlier works,[3,14] until the puzzle was finally explained by Sarkis and Callen.[15]

In total, there have been two independent treatments[3,4] of the same neutron data set (Table I, upper part) and as many as four attempts[5,8–10] to determine model parameters from the magnetization data of Refs. 5 and 6 (Table I, lower part). No consistent values were deduced from either data set.

In a previous work,[16] we proposed a method of determining $H_{\rm mol}$ from high-field magnetization data. The method produced consistent results for $Er_2Fe_{17}$.[16] Since $Ho_2Fe_{17}$ is an easy-plane ferrimagnet, the same technique suits it ideally. So we decided to carry out a high-field magnetization study of $Ho_2Fe_{17}$ in order to determine $H_{\rm mol}$ more accurately and to find out why the previous experiments on $Ho_2Fe_{17}$ single crystals failed to determine even the order of magnitude of $K_4^{\rm Ho}$. This work is organized as follows. In the next section, a brief description of the experimental procedure and of the equipment used is given, most notably of the high-field magnetometer. Section III presents the results of the measurements. The theoretical model is stated in Sec. IV, some of the details being relegated to the Appendices. Section V contains a discussion, a determination of $H_{\rm mol}$, an estimation of $K_4^{\rm Ho}$, and a conclusion.

## II. EXPERIMENTAL DETAILS

The samples were prepared by induction melting of mixtures of 99.9%-pure Ho and 99.99%-pure Fe in alundum crucibles under an Ar atmosphere. The mixture of the nominal molar ratio 2:17 was rapidly melted, then cooled down to room temperature at a rate of 100 °C/min. The obtained ingot was annealed in a resistive furnace under a vacuum as follows. It was heated up to 1300 °C during 1 h and kept at this

 

TABLE I. Published values of the crystal field parameter $A_6^6\langle r^6\rangle$ and of the anisotropy constant $K_4^{Ho}$ of $Ho_2Fe_{17}$.

| $A_6^6\langle r^6\rangle$ (K) | $K_4^{Ho}$ (J/kg) |
|---|---|
| −68[a] | 100 |
| −9[b] | 14 |
| – | 200[c] |
| −190[d] | 290 |
| −104[e] | 170 |
| −22[f] | 33 |

[a]Ref. 3
[b]Ref. 4
[c]Refs. 5 and 6
[d]Ref. 8
[e]Ref. 9
[f]Ref. 10

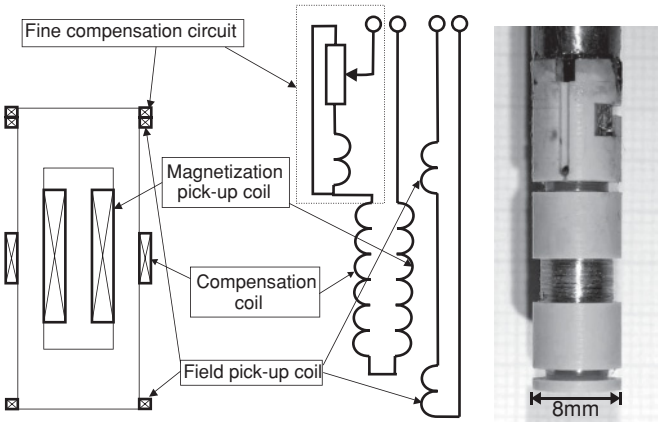


FIG. 1. Pickup-coil system used in the pulsed-field magnetometer with (Left) the principal sketch, (Middle) the electrical scheme, and (Right) a picture of the original set up.

temperature for 10 min in order to melt. Then, it was cooled down to 1150 °C during 1 h and kept there for 8 h. This mode is favorable for growth of large crystalline grains. The phase composition of the ingot was checked by means of optical metallography, x-ray phase analysis, and energy-dispersive x-ray spectroscopy. The ingot was then broken down by ultrasound, and large grains were picked out. The so-obtained specimens were subject to mechanical shaping by rough and coarse grinding. Besides forming the sample spherically, which is a preferred shape for magnetization measurements, this procedure helps to reject twinned crystals as they would not stand high mechanical stress. The stressed surface was relaxed by electropolishing in a $CrO_3$ solution. The final single-crystallinity test and orientation of the samples were performed by means of x-ray back Laue diffraction.

Magnetization measurements were performed at the Dresden High Magnetic Field Laboratory.[17] The pulsed coil used in this work has been described elsewhere.[18] A single 1.44 MJ capacitor module was used. The capacitor module was charged to 22 kV and delivered a peak current of about 30 kA. This produced a maximum magnetic field of 60 T with a rise time of about 7 ms and a total pulse duration of 25 ms. (The coil design provided for nondestructive operation at fields up to 65 T.)

The magnetic field was measured by two coils connected in series and located above and below the sample pickup coils (Fig. 1). In order to avoid a possible influence of the sample on the field measurement, the coils were placed reasonably far from the sample position. The signal from the coils, proportional to $\dot{H} \equiv (dH/dt)$, was recorded by a digitizer and later integrated numerically. The pickup-coil signal was calibrated by measuring the well-known magnetization curve of $MnF_2$, where a temperature-independent spin-flop transition takes place at 9.27 T.[19]

The magnetization was measured by a pickup coil surrounding the sample. Since the coil is situated in a varying magnetic field, it should be connected to a compensation coil canceling the $\dot{H}$ contribution. Several arrangements of the compensated pickup-coil system are possible. We have chosen a coaxial geometry as it is less sensitive to gradients and vibrations. The pickup coil consists of 1200 turns wound around a 3.2 mm diameter sample space and is 5 mm long. The compensating coil was wound around a 6.8 mm diameter support. It was realized with a somewhat larger effective area then the pickup coil, the final compensation was performed by taking windings off the compensation coil to null the overall signal. This procedure resulted in a compensation of about $2 \times 10^{-3}$. The remaining temperature-dependent part was further reduced at each temperature by a fine-compensation circuit using an additional coil (Fig. 1). The housing of the magnetometer was made out of plastic (PEEK) with a very low thermal expansion. The sample was placed in the coil system without taking the magnetometer out of the cryostat (top-loading system). Each measurement of the sample was complemented by recording the background in identical conditions and its subsequent subtraction. The absolute value of the magnetization was calibrated by a low-field measurement using a commercial superconducting quantum interference device (SQUID) magnetometer.

The measurement of an unclamped sample was performed at the Dresden Leibniz Institute for Materials Science (IFW). In that case, two identical 3-mm-long pickup coils were placed side by side, one of them containing the sample. The inner bore diameter of the coils was 1 mm. The sample was approximately a sphere, about 0.7 mm in diameter. Two plastic pistons restricted the translational motion of the sample, while leaving it free to rotate. For more details on the free-rotation technique, see Ref. 16.

## III. RESULTS

Figure 2 displays the magnetization of $Ho_2Fe_{17}$ measured at 4.3 K for three crystallographic directions (solid lines). The data measured along [001] clearly identifies this as a hard magnetization direction. There is no component of spontaneous magnetization along [001], which confirms good crystal quality and orientation. A small spontaneous moment along [001] was reported for one sample in Ref. 6 but was not observed on another crystal.[10] Comparing the [100] and [120] directions, one observes an in-plane magnetic anisotropy, with [120] being the easy direction. According to our data, the spontaneous magnetization of $Ho_2Fe_{17}$ is $18.2\,\mu_B$/f.u. at $T = 4.3$ K. The literature data scatter significantly: Clausen and Nielsen

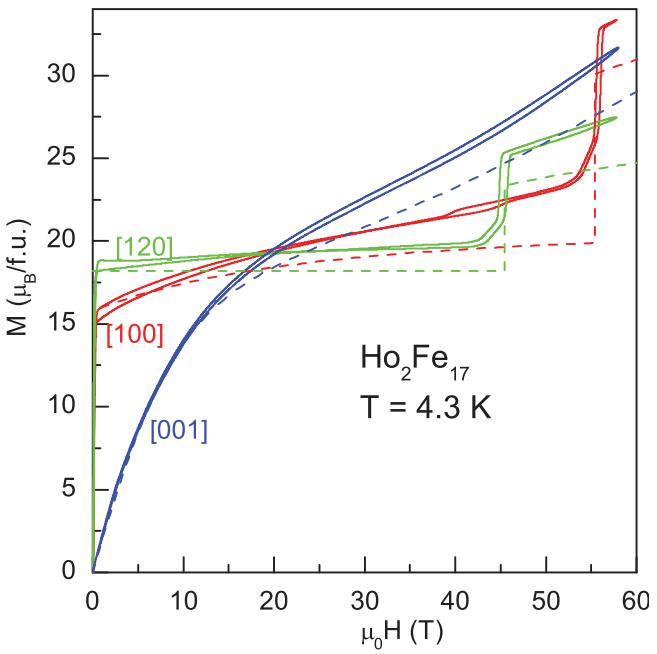


FIG. 2. (Color online) Magnetization curves of $Ho_2Fe_{17}$ measured along the main crystallographic directions at 4.3 K. Solid and dashed lines are experimental and calculated data, respectively.

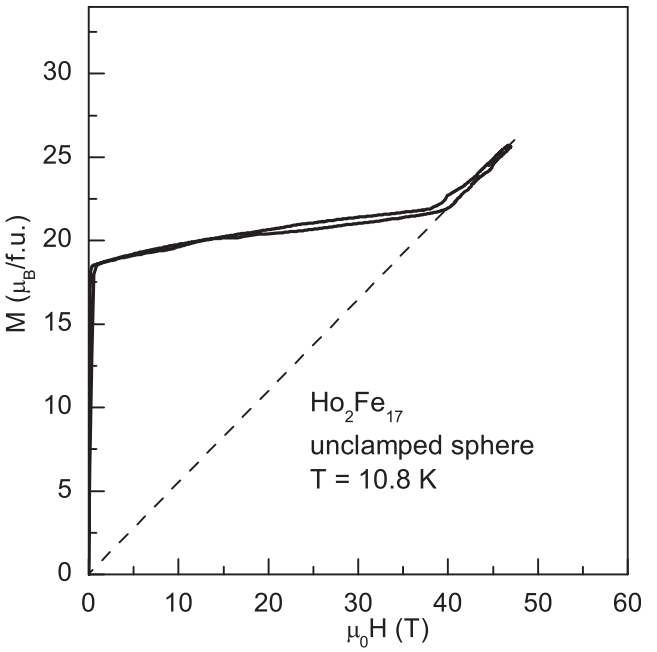


FIG. 3. Magnetization curve measured on an unclamped single crystal of $Ho_2Fe_{17}$.

reported 16.36 $\mu_B$/f.u.,[14] Sinnema found 18.6 $\mu_B$/f.u.,[5,6] and Tereshina *et al.* derived 18.8 $\mu_B$/f.u.[20] First-order transitions are evident in the magnetization data measured along the [100] and [120] directions at 56 and 45.5 T, respectively. The corresponding heights of the jumps are 8.4 and 5.6 $\mu_B$/f.u.

Following Ref. 21, we attribute the jumps to stepwise reorientation of the rare-earth moment between adjacent easy directions within the basal plane. In the limit of strong anisotropy, relevant also to $Ho_2Fe_{17}$, three or two jumps must take place, depending on whether the field is applied along an easy or a hard direction in the basal plane. Every abrupt rotation of $\boldsymbol{M}_{\mathrm{Ho}}$ through $\pi/3$ recoils upon $\boldsymbol{M}_{\mathrm{Fe}}$, so that both sublattice moments reorientate discontinuously.

The magnetization of the unclamped sample is presented in Fig. 3. The low-field part of the curve agrees well with the fixed-sample data of Fig. 2 taken in the easy magnetization direction [120]. At 40 T, there is a well-pronounced kink corresponding to the beginning of continuous rotation of $\boldsymbol{M}_{\mathrm{Ho}}$ and $\boldsymbol{M}_{\mathrm{Fe}}$. Beyond that point, the [120] axis of the unclamped crystal stays no longer parallel to the magnetic field, but rather is involved in the coordinated rotation of the sublattice moments. The high-field part of the curve roughly extrapolates to the origin.

## IV. THEORY

In order to describe quantitatively the low-temperature magnetization of $Ho_2Fe_{17}$, we make use of the two-sublattice model of Ref. 16. We are interested primarily in a special case when the applied field is perpendicular to the sixfold axis of the crystal—that is, when the field-induced first-order transitions are observed. The easy-plane ferrimagnet $Ho_2Fe_{17}$ is particularly suitable for such orientations of an applied magnetic field because then all the magnetic moments remain in the basal plane and the model[16] yields unambiguous predictions. The starting point of the model (limited to the special case $\boldsymbol{H} \perp [001]$) is the following thermodynamic potential:

$$\Phi = \lambda M_{\mathrm{Fe}} M_{\mathrm{Ho}} \cos(\alpha+\beta) - H M_{\mathrm{Fe}} \cos\alpha - H M_{\mathrm{Ho}} \cos\beta \pm \left|K_4^{\mathrm{Ho}}\right| \cos 6\beta. \quad (2)$$

Here, $M_{\mathrm{Fe}}$ and $M_{\mathrm{Ho}}$ are magnetizations of the two sublattices, $\lambda$ is the intersublattice exchange constant ($\lambda > 0$), $\alpha$ and $\beta$ are angles between the magnetic field $\boldsymbol{H}$ and the vectors $\boldsymbol{M}_{\mathrm{Fe}}$ and $\boldsymbol{M}_{\mathrm{Ho}}$, respectively, and $K_4^{\mathrm{Ho}}$ is the basal-plane anisotropy constant of the Ho sublattice. (The basal-plane anisotropy of the Fe sublattice is negligible.) The signs "+" or "−" correspond, respectively, to the orientation of the applied field along a hard or an easy direction within the basal plane.

Following Ref. 16, we introduce dimensionless variables,

$$h = \frac{H}{\lambda M_{\mathrm{Fe}}}, \quad \phi = \frac{\Phi}{\lambda M_{\mathrm{Fe}}^2}, \quad \kappa = \frac{\left|K_4^{\mathrm{Ho}}\right|}{\lambda M_{\mathrm{Fe}}^2}, \quad m = \frac{M_{\mathrm{Ho}}}{M_{\mathrm{Fe}}}, \quad (3)$$

and rewrite the thermodynamic potential [Eq. (2)] as follows:

$$\phi = m\cos(\alpha+\beta) - h\cos\alpha - mh\cos\beta \pm \kappa\cos 6\beta. \quad (4)$$

The process of generating magnetization curves consists in minimizing the potential [Eq. (4)] with respect to the angles $\alpha$ and $\beta$ for a given field $h$ and setting the obtained equilibrium values of $\alpha$ and $\beta$ into an expression for reduced magnetization:

$$\sigma = \frac{\cos\alpha + m\cos\beta}{1-m}. \quad (5)$$

The reduced magnetization is normalized to unity in weak magnetic fields ($h \to 0, \alpha \to 0, \beta \to \pi$).

Obviously, the shape of the curves $\sigma(h)$ depends on two parameters, $m$ and $\kappa$. The value of $m$ is readily found by setting $M_{\mathrm{Ho}}$ to twice the free-ion moment, i.e., 20 $\mu_B$/f.u.

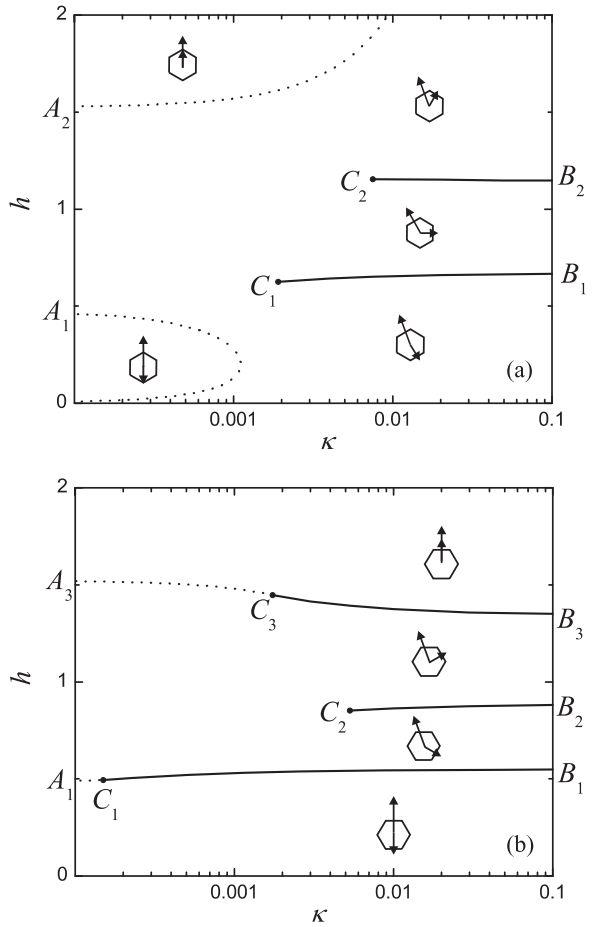


FIG. 4. Phase diagram of an easy-plane hexagonal ferrimagnet with $m = 0.524$. The magnetic field is applied (a) in the hard or (b) in the easy direction in the basal plane. Solid and dotted lines are first- and second-order phase transition lines, respectively. In the pictograms, the longer arrows correspond to $\boldsymbol{M}_{\mathrm{Fe}}$ and the shorter ones to $\boldsymbol{M}_{\mathrm{Ho}}$; the magnetic field (not shown) is directed upward.

Then, from the spontaneous magnetization, $M_s = M_{\mathrm{Fe}} - M_{\mathrm{Ho}} = 18.2\,\mu_B$/f.u., we obtain $M_{\mathrm{Fe}} = 38.2\,\mu_B$/f.u. and $m = M_{\mathrm{Ho}}/M_{\mathrm{Fe}} = 0.524$. As against that, the anisotropy parameter $\kappa$ is not known a priori. In order to get an overview of all possible $\sigma(h)$ dependences, it is instructive, following Ref. 16, to describe the behavior of the entire class of systems with a given $m$ but different $\kappa$ by means of phase diagrams in the $\kappa$-$h$ plane. Such diagrams for $Ho_2Fe_{17}$ ($m = 0.524$) are presented in Fig. 4, where the upper panel (a) corresponds to the magnetic field being parallel to a hard direction in the basal plane [plus sign in Eq. (4)], and the lower panel (b) to an easy direction within the basal plane. The latter case was analyzed in detail in Ref. 16, dedicated to $Er_2Fe_{17}$. It is immaterial that the easy direction in $Er_2Fe_{17}$ is the crystallographic $a$ axis [100], whereas in $Ho_2Fe_{17}$, it is the $b$ axis [120]. The difference between Fig. 4(b) of the present work and Fig. 5 of Ref. 16 is merely quantitative, due to a slightly different $m$. Explicit expressions for the coordinates of the key points in this phase diagram at any $m$, obtained in Ref. 16, are given in Appendix A.

Here, we will concentrate on the former case ($\boldsymbol{H}$ || hard direction in the basal plane), Fig. 4(a), which has not been studied before. Figure 5 displays several representative magnetization curves $\sigma(h)$ relevant to this case. Each such curve, computed at a certain fixed $\kappa$, corresponds to a vertical line in Fig. 4(a). Where such a line crosses a solid/dotted phase separation line in Fig. 4(a), a first-/second-order phase transition, respectively, takes place. Such a transition corresponds to a jump/kink in Fig. 5 so that the ordinate of the crossing point in Fig. 4(a) is the threshold field of the transition in Fig. 5. Explicit expressions for $\sigma(h)$ can only be obtained in special cases of $\kappa = 0$ and $\kappa = \infty$. In the former case, $\sigma(h)$ is given by the following expression [Eq. (6) in Ref. 16, derived earlier in Refs. 22 and 23] regardless of the orientation of the field in the basal plane:

$$\sigma(h) = \begin{cases} 1 & \text{if} \quad h < 1 - m \\ \frac{h}{1-m} & \text{if} \quad 1 - m < h < 1 + m \\ \frac{1+m}{1-m} & \text{if} \quad h > 1 + m. \end{cases} \tag{6}$$

In a weak magnetic field ($h < 1 - m$), the system is a collinear ferrimagnet, at intermediate fields it has a canted magnetic structure, and above $h = 1 + m$, it is a (forced) ferromagnet. At $h = 1 \pm m$, second-order transitions take place; these are seen as kinks in the magnetization curve in Fig. 5(a). For $\kappa = \infty$, we obtained the following expression:

$$\sigma(h) = \frac{1}{1-m} \times \begin{cases} \dfrac{h + \frac{1}{2}\sqrt{3}m}{\sqrt{\left(h + \frac{1}{2}\sqrt{3}m\right)^2 + \frac{1}{4}m^2}} - \frac{\sqrt{3}}{2}m & \text{if} \quad h < h_1 \\ \dfrac{h}{\sqrt{h^2 + m^2}} & \text{if} \quad h_1 < h < h_2 \\ \dfrac{h - \frac{1}{2}\sqrt{3}m}{\sqrt{\left(h - \frac{1}{2}\sqrt{3}m\right)^2 + \frac{1}{4}m^2}} + \frac{\sqrt{3}}{2}m & \text{if} \quad h > h_2, \end{cases} \tag{7}$$

where

$$h_{1,2} = \frac{\sqrt{3m^4 + 16(1 - m^2)} \pm \sqrt{3}m}{4 - \frac{3}{4}m^2}. \tag{8}$$

The three field intervals in Eq. (7) correspond to three distinct phases, characterized by three different values of the angle $\beta$ between $\boldsymbol{M}_{\mathrm{Ho}}$ and $\boldsymbol{H}$. In the low-field phase, $\boldsymbol{M}_{\mathrm{Ho}}$ makes an obtuse angle with $\boldsymbol{H}$, $\beta = 5\pi/6$. In the intermediate

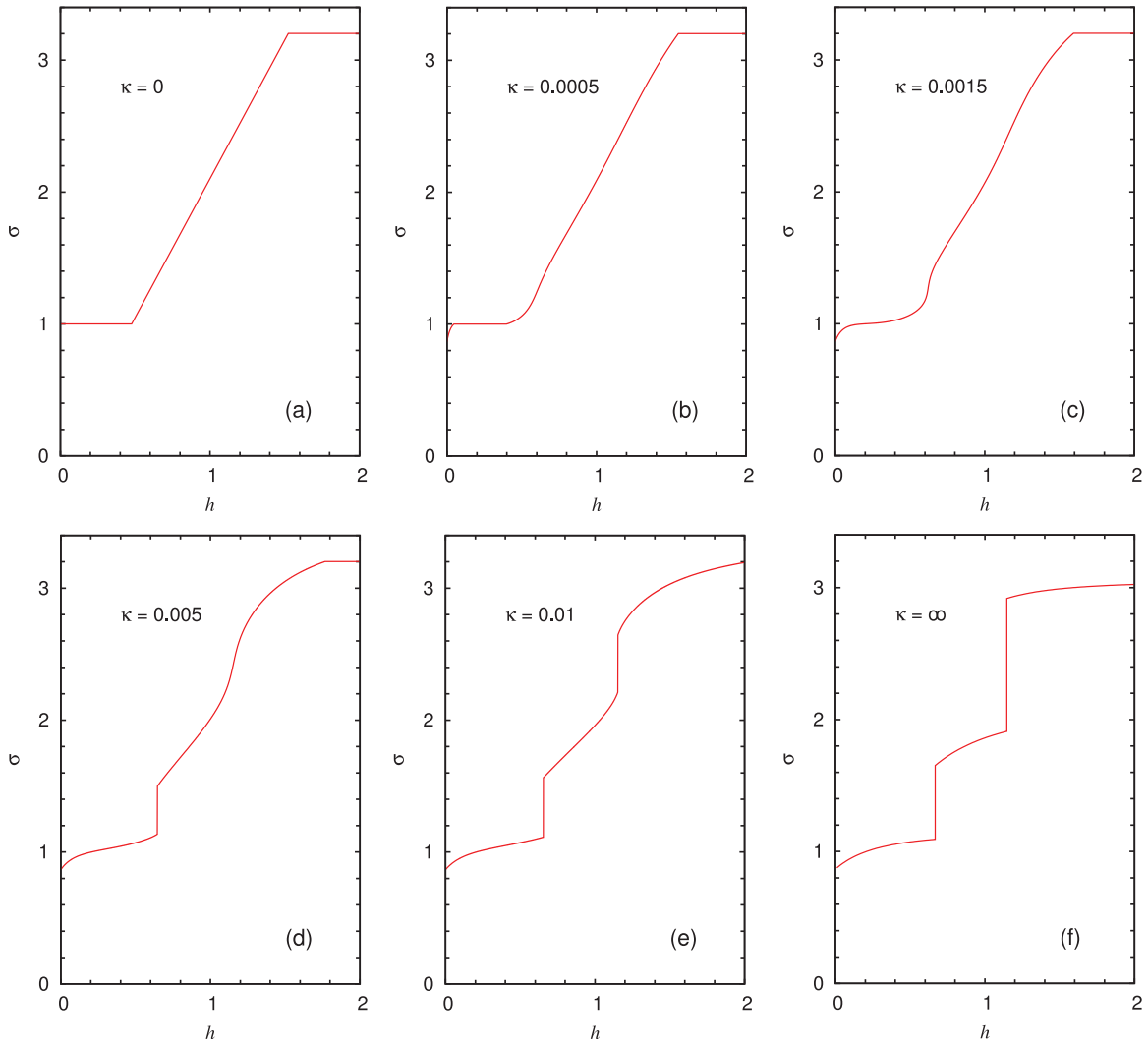


FIG. 5. (Color online) Representative magnetization curves for $m = 0.524$ and applied magnetic field pointing in the hard direction in the basal plane.

phase, $\boldsymbol{M}_{\mathrm{Ho}}$ is perpendicular to $\boldsymbol{H}$, and in the high-field phase, $\boldsymbol{M}_{\mathrm{Ho}}$ and $\boldsymbol{H}$ make an acute angle, $\beta = \pi/6$. In all the cases, $\boldsymbol{M}_{\mathrm{Ho}}$ takes one of the crystallographically equivalent easy directions within the basal plane. Transitions between the phases take place at $h = h_1$ and $h = h_2$ and are first-order phase transitions. They correspond to discontinuities (jumps) in the magnetization curve [Fig. 5(f)].

At intermediate values of the anisotropy parameter $\kappa$, $\sigma(h)$ has to be calculated numerically, yet the positions of all key points as well as the dotted lines in the phase diagram [Fig. 4(a)] are given by simple expressions (see Appendix B).

In the case of a very weak anisotropy, $\kappa < \frac{1}{36}m(1-\sqrt{m})^2$, the locus of the system in the phase diagram crosses the dotted lines three times, according as the field $h$ grows. Consequently, three field-induced second-order transitions take place and the magnetization curve has three kinks [Fig. 5(b)]. Within the initial growing portion of the curve, rotation of both sublattice vectors, $\boldsymbol{M}_{\mathrm{Fe}}$ and $\boldsymbol{M}_{\mathrm{Ho}}$, takes place, their antiparallel mutual orientation being maintained to a significant extent. The vector $\boldsymbol{M}_{\mathrm{Fe}}$ turns from its initial position at $\alpha = \pi/6$ toward the magnetic field, becoming parallel to it at the transition point. At the same time, $\boldsymbol{M}_{\mathrm{Ho}}$ rotates from $\beta = 5\pi/6$ away from the field and becomes antiparallel to the latter at the transition point. The first transition takes place when the locus of the system crosses the lower part of the dotted hyperbolic arc in the southwest corner of the phase diagram [Fig. 4(a)]. Above the transition point, the orientation of the vectors $\boldsymbol{M}_{\mathrm{Ho}}$ and $\boldsymbol{M}_{\mathrm{Fe}}$ does not change, and the system is a collinear ferrimagnet. As the applied field grows, the magnetization remains constant, $\sigma \equiv 1$, until the second threshold point is reached. Now, the locus of the system crosses the upper part of the dotted hyperbolic arc in Fig. 4(a), and the magnetization $\sigma(h)$ resumes its growth. The orientation of the sublattice moments starts to change again. The angle $\beta$ between $\boldsymbol{M}_{\mathrm{Ho}}$ and $\boldsymbol{H}$ decreases monotonically from $\pi$ to 0. The angle $\alpha$ between $\boldsymbol{M}_{\mathrm{Fe}}$ and $\boldsymbol{H}$ changes nonmonotonically: it grows at first from 0 to a certain maximum value, then it decreases down to 0. The mutual orientation of the sublattice moments changes gradually and monotonically from antiparallel to parallel. The parallel orientation of all three vectors, $\boldsymbol{M}_{\mathrm{Ho}}$, $\boldsymbol{M}_{\mathrm{Fe}}$, and $\boldsymbol{H}$, is attained at the third threshold field, as the system's locus crosses the upper dotted hyperbola in Fig. 4(a).

Thereupon, the magnetization ceases to grow definitively and is saturated.

According as the anisotropy parameter $\kappa$ grows, the intermediate-field horizontal portion of the magnetization curve becomes ever more narrow, until it disappears altogether. This happens when the locus of the system passes through the vertex of the hyperbolic arc in Fig. 4(a), situated at $\kappa = \frac{1}{36}m(1-\sqrt{m})^2$ and $h = \sqrt{m} - m$. For larger $\kappa$, the collinear ferrimagnetic state is never attained, and the magnetization curve has only one kink corresponding to the transition into the forced ferromagnetic state (spin flip) [see Fig. 5(c)]. The spin flip occurs when the system's locus in the phase diagram [Fig. 4(a)] reaches the the high-field dotted hyperbola.

As $\kappa$ increases further, the S-shaped anomaly in the magnetization curves develops into a discontinuity [Fig. 5(d)]. At yet larger $\kappa$, a second S-shaped anomaly appears at a higher field, which eventually also turns into a discontinuity [Fig. 5(e)]. The two discontinuities appear when the system's locus in the phase diagram reaches the critical points $C_1$ and $C_2$, respectively, i.e., at $\kappa = \frac{1}{48}m^2(1-\frac{1}{2}m^2 \pm m\sqrt{1-\frac{3}{4}m^2})$. A derivation of this expression, as well as a summary of the positions of the main points and lines of the phase diagram of Fig. 4(a), is given in Appendix B. From the physical viewpoint, the jumps in the magnetization occur when the vector $\boldsymbol{M}_{\mathrm{Ho}}$ passes through a hard direction in the basal plane, as it rotates toward the magnetic field. At small $\kappa$, overcoming the barrier associated with the anisotropy proceeds as a continuous process; however, starting from certain critical values of the anisotropy parameter, discontinuities appear. This does not happen simultaneously; first, the position of $\boldsymbol{M}_{\mathrm{Ho}}$ near $\beta = 2\pi/3$ becomes unstable, then near $\beta = \pi/3$.

A further increase of $\kappa$ does not lead to any qualitative change in the $\sigma(h)$ curves. They still have two discontinuities, only the height of the jumps grows with $\kappa$. At the same time, the change of slope (kink) associated with the spin flip moves to higher fields, becoming ever less noticeable. As a matter of fact, starting from about $\kappa = 0.1$, the magnetization curves are indistinguishable from those with $\kappa = \infty$.

## V. DISCUSSION

The theory developed in Ref. 16 and complemented in Sec. IV suggests a simple explanation for the enigmatic situation surrounding the basal-plane anisotropy constant $K_4^{\mathrm{Ho}}$. According to this theory, the height of the first jump of magnetization in the easy direction grows with $\kappa$, tending to a certain limit as $\kappa \to \infty$,[16]

$$\Delta\sigma_1 = \frac{m(1-m/4)}{2-m+m^2/2} = 0.282, \tag{9}$$

where $m = 0.524$ has been used. From our experimental magnetization curve along [120], we deduce $\Delta\sigma_1 = 0.31$, that slightly exceeds the theoretical upper bound [Eq. (9)]. The discrepancy is not significant, considering the already mentioned uncertainty of the spontaneous moment and, therefore, of the parameter $m$. Still, in order to reconcile the model with the experiment in the best possible way, one has to conclude that the system operates in the strong-anisotropy regime, when the magnetization curves no longer depend on $\kappa$. The advantage of this situation is that one can use explicit expressions for $\sigma(h)$, Eq. (7) of this work for $\boldsymbol{H}||[100]$ and Eq. (7) of Ref. 16 for $\boldsymbol{H}||[120]$. Yet, one has to accept that $\kappa$ cannot be determined from the available magnetization data. Having at our disposal the height of the first jump, we cautiously estimate that

$$\kappa \gtrsim 0.02, \text{ or} K_4^{\mathrm{Ho}} \gtrsim 3\times 10^2\ \mathrm{J/kg}. \tag{10}$$

We are unable to put any upper limit on $\kappa$ or $K_4^{\mathrm{Ho}}$ at this point. Yet, values significantly smaller than the estimated lower bound (10) can be ruled out.

According to Eq. (A2), the dimensionless critical field of the first jump equals 0.548 for $\boldsymbol{H}||[120]$. Experimentally, it is observed at 45.5 T. Hence, for the molecular field on Ho, we find

$$\mu_0 H_{\mathrm{mol}} = \lambda M_{\mathrm{Fe}} = \frac{45.5\,\mathrm{T}}{0.548} = 83\,\mathrm{T}. \tag{11}$$

For $\boldsymbol{H}||[100]$, the critical field of the first jump is obtained from Eq. (8), lower sign: $h_1 = 0.667$. This is converted to teslas using the value [Eq. (11)] as a scaling factor: $\mu_0 H_1 = 0.667\times 83.0 = 55.4$ T. This prediction is in good agreement with the experiment (Fig. 2). Similarly, from Eqs. (A3) and (A2), we predict two further jumps at 73 and 112 T for $\boldsymbol{H}||[120]$, and from Eq. (8), a jump at 95 T for $\boldsymbol{H}||[100]$. (In earlier calculations,[21] the critical fields came out systematically higher: 46, 97, and 135 T for $\boldsymbol{H}||[120]$ and 62 and 125 T for $\boldsymbol{H}||[100]$.) Finally, the value [Eq. (11)] and the spontaneous moment, $M_s = 18.2\,\mu_B$/f.u., can be used to convert into absolute units the magnetization curves along [100] and [120], as given by Eq. (7) of this work and Eq. (7) of Ref. 16, respectively. The results are shown as dashed lines in Fig. 2.

To complete the picture, one still needs a theoretical magnetization curve for the third principal direction [001]. Since the experimental curve is rather featureless, a very simple model may be adopted. The anisotropy of the iron sublattice is neglected completely, whereas for holmium just the leading anisotropy constant $K_1^{\mathrm{Ho}}$ is allowed for. There is no physical reason to believe that at $T \sim 4$ K, $K_2^{\mathrm{Ho}}$ or $K_3^{\mathrm{Ho}}$ is much smaller than $K_1^{\mathrm{Ho}}$. Moreover, the curve will be definitely affected by $K_4^{\mathrm{Ho}}$, even taken at its lower bound (10). Yet, the available data do not suffice for a unique determination of all four relevant anisotropy constants, so these are replaced by a single "effective" second-order anisotropy constant $K_1^{\mathrm{Ho}}$. The advantage of such an approximation is the possibility of expressing the magnetization curve in parametric form:[24]

$$h = \frac{m}{m+\kappa_1 t}\sqrt{\frac{1-(m+\kappa_1 t)^2}{1-mt}}, \tag{12}$$

$$\sigma = \frac{h}{1-m}\left(1+\frac{\kappa_1}{m}t-\frac{\kappa_1}{2}t^2\right), \tag{13}$$

with

$$\kappa_1 = \frac{K_1^{\mathrm{Ho}}}{\lambda M_{\mathrm{Fe}}^2}. \tag{14}$$

The parameter $t$ runs from a negative initial value, $t_0 = (1-m)/\kappa_1$, which corresponds to $h = \sigma = 0$, to a certain positive

upper bound corresponding to full saturation. The initial slope, $\chi_0 = (\partial\sigma/\partial h)_{h=0}$, is given by

$$\chi_0 = \frac{1}{m(1-m)} - \frac{1-m}{2\kappa_1}. \tag{15}$$

From our experimental data we deduce $\chi_0 = 8.6$, then from Eq. (14) we find $\kappa_1 = 0.052$. This value is set into Eqs. (12) and (13), which are now fully defined. The resulting magnetization curve, upon appropriate conversion of units, is presented in Fig. 2 (dashed line).

Comparing the experimental (solid) and calculated (dashed) magnetization curves in Fig. 2, one observes that the latter progressively "fall behind" the former. This is the case for all orientations of applied magnetic field to roughly the same extent. The lag does not affect the threshold fields or relative heights of the magnetization jumps, which are well reproduced by the calculations. At present, we are not in a position to explain the provenance of the growing background in the magnetization curves. A magnetization growth may take place for several reasons, e.g., because the crystal is twinned, or it may be that the iron sublattice magnetization increases with magnetic field. The twinning does not appear likely since the observed magnetization jumps have the full expected heights and no satellites. If one could induce a transition into a forced ferromagnetic state, it would be very interesting to compare the magnetization with the sum of the sublattice moments in our model, $58.2\mu_B$/f.u., and to measure the differential susceptibility above the transition. Unfortunately, the required field, 112 T, applied in the easy direction [120] is presently not attainable in experiments of this kind, where sufficient pulse duration is essential. Under the circumstances, we took a different approach to checking our interpretation of the data. Our attention turned to the previously determined molecular field on Ho [Eq. (11)]. For verification, we carried out magnetization measurements on a free-to-rotate single-crystalline sphere of $Ho_2Fe_{17}$. The magnetization (Fig. 3) has a clearly visible kink at 40 T. The analysis of this experiment is particularly simple because it is equivalent to the well-studied isotropic case.[23] The critical field of the kink equals $\lambda(M_{Fe} - M_{Ho})$, whence it follows that

$$\mu_0 H_{mol} = \frac{M_{Fe}}{M_{Fe} - M_{Ho}} \mu_0 H_{kink} = \frac{38.2}{18.2} \times 40\,\mathrm{T} = 84\,\mathrm{T}. \tag{16}$$

This agrees with the value [Eq. (11)] deduced from the data taken on a fixed crystal and confirms the soundness of our model. For comparison, the value found by Sinnema[5,6], $\mu_0 H_{mol} = 88$ T, is somewhat too high, whereas Clausen and Lebech[4] obtained a far too low value, $\mu_0 H_{mol} = 58.5$ T. The reason for the discrepancy is that the neutron-scattering data[3,4] do not allow to determine $H_{mol}$ independently from the crystal-field parameters, and the latter were severely misjudged in Refs. 3 and 4 (the two values of $A_6^6\langle r^6\rangle$ at the top of Table I were deduced from the same data set).

Coming back to the anisotropy constants, one might be tempted by the idea of determining them from a fit to the magnetization curve along the sixfold axis [001]. It should be noted that allowing for higher-order anisotropy constants in Eqs. (12) and (13) is not possible. Even if it were, it would be pointless since higher-order anisotropy constants cannot in principle improve the fit. Irrespective of the anisotropy, the calculated curve must pass through the so-called orthogonality point, whose coordinates are:[25] $H_\perp = H_{mol}\sqrt{1-m^2} = 70.7$ T and $M_\perp = \sqrt{M_{Fe}^2 - M_{Ho}^2} = 32.5\,\mu_B$/f.u. All that can be reasonably extracted from the rather smooth experimental curve is its initial slope. Unlike Eqs. (12) and (13), Eq. (15) can be readily generalized to include higher-order anisotropy constants. It suffices to replace the parameter $\kappa_1$ defined by Eq. (14) with the following quantity,

$$\frac{K_1^{Ho} + 2K_2^{Ho} + 3K_3^{Ho} - 3K_4^{Ho}}{\lambda M_{Fe}^2}, \tag{17}$$

which by virtue of our data must equal $-0.052$. The dominant contribution to Eq. (15) seems to come from $K_4^{Ho}$; cf. the estimates (10). In this situation, little can be said with certainty about $K_1^{Ho}$, $K_2^{Ho}$, or $K_3^{Ho}$. This conclusion applies to all currently available data. Determining $K_1^{Ho}$ and $K_2^{Ho}$ may well become possible in the future, when the [001] curve is measured to saturation, i.e., to the transition into the forced ferromagnetic state (spin flip). The critical field of the transition $H_{flip}$ would enable one to find $K_1^{Ho}$ from Eq. (20) of Ref. 25, and $K_2^{Ho}$ could then be found from the slope of the curve just before the transition [Eq. (41) of Ref. 24].

As regards $K_4^{Ho}$, we do not expect it to be significantly higher than the estimated lower bound (10), since, otherwise, an unlikely near cancellation of terms in (17) must take place. Therefore, $K_4^{Ho} \sim 3 \times 10^2$ J/kg can be adopted as an order-of-magnitude estimate.

In conclusion, stepwise anomalies in the high-field magnetization curves of $Ho_2Fe_{17}$ have been observed at 45 T for $\boldsymbol{H}||[120]$ as well as at 55 T for $\boldsymbol{H}||[100]$. Further such anomalies are expected at 73 and 112 T for $\boldsymbol{H}||[120]$ and at 95 T for $\boldsymbol{H}||[100]$. The molecular field on the Ho sublattice has been found to be about 83 or 84 T, whereas no precise anisotropy constants could be deduced from the data available so far.

## ACKNOWLEDGMENTS

Part of this work has been supported by EuroMagNET under EU Contract No. 228043. A.V.A. thanks for support Research Project No. AVOZ10100520 and Grant No. 09/202/0339 of the Czech Science Foundation.

## APPENDIX A: PHASE DIAGRAM FOR A MAGNETIC FIELD APPLIED ALONG AN EASY DIRECTION IN THE BASAL PLANE

This is a summary of the main facts—coordinates of key points and equations of phase boundaries—concerning the phase diagram of Fig. 4(b). All these results were obtained earlier[16] and are given here without proof. Where two objects are described by a single equation with double signs, the upper signs always correspond to the object named first.

The ordinates of the points $A_1$ and $A_3$ on the left-hand edge of the diagram (at $\kappa = 0$) are

$$h = 1 \mp m. \tag{A1}$$

The ordinates of the infinitely remote points $B_1$ and $B_3$ on the right of Fig. 4(b) are

$$h = \frac{1 \mp m}{1 \mp m/4}. \tag{A2}$$

The ordinate of the infinitely remote point $B_2$ is

$$h = \sqrt{\frac{1-m^2}{1-m^2/4}}. \tag{A3}$$

The coordinates of the tricritical points $C_1$ and $C_3$ are

$$\kappa = \mp \frac{mh}{36}\left(\frac{1}{h \pm m} - 1\right), \tag{A4}$$

where

$$h = \frac{1}{3} \mp m + \frac{2}{3}\sqrt{1 \pm \frac{9}{35}m} \times \cos\left[\frac{1}{3}\arccos\frac{1 \pm \frac{27}{70}m - \frac{81}{70}m^2}{\left(1 \pm \frac{9}{35}m\right)^{3/2}}\right]. \tag{A5}$$

The coordinates of the tricritical point $C_2$ are

$$\kappa = \tfrac{1}{36}m^2(1-m^2), \tag{A6}$$

$$h = \sqrt{1-m^2}. \tag{A7}$$

The lines $B_1C_1$ and $B_3C_3$ are given by

$$h = \sqrt{\left(\frac{1 \mp m}{2} \pm \frac{18\kappa}{m}\right)^2 + 36\kappa} + \frac{1 \mp m}{2} \pm \frac{18\kappa}{m}. \tag{A8}$$

## APPENDIX B: PHASE DIAGRAM FOR A MAGNETIC FIELD APPLIED ALONG A HARD DIRECTION IN THE BASAL PLANE

### 1. Phase boundary of the forced ferromagnetic state

Let us write down the necessary conditions for a minimum, $\partial\phi/\partial\alpha = \partial\phi/\partial\beta = 0$, for Eq. (4), choosing the plus sign in front of $\kappa$ therein:

$$-m\sin(\alpha+\beta) + h\sin\alpha = 0, \tag{B1}$$

$$-m\sin(\alpha+\beta) + mh\sin\beta - 6\kappa\sin 6\beta = 0. \tag{B2}$$

Regarding the angles $\alpha$ and $\beta$ as small quantities, we omit the sine symbols from Eqs. (B1) and (B2):

$$(h-m)\alpha - m\beta = 0, \tag{B3}$$

$$-m\alpha + (mh - m - 36\kappa)\beta = 0. \tag{B4}$$

In order for these simultaneous linear equations to have a nontrivial solution, their determinant must be nil. Therefore,

$$\kappa = \frac{mh}{36}\left(\frac{1}{m-h} + 1\right). \tag{B5}$$

This equation describes the dotted hyperbola in the upper part of Fig. 4(a). Equation (B5) can be readily rewritten in explicit form, as $h$ versus $\kappa$:

$$h = \sqrt{\left(\frac{1+m}{2} + \frac{18\kappa}{m}\right)^2 - 36\kappa} + \frac{1+m}{2} + \frac{18\kappa}{m}. \tag{B6}$$

Note that the same result is obtained by changing the sign of $\kappa$ in Eq. (A8) taken with the lower signs.

### 2. Line delimiting the domain of stability of the collinear ferrimagnetic phase

This is obtained by substitution of $-m$ for $m$ in Eq. (B5):

$$\kappa = \frac{mh}{36}\left(\frac{1}{m+h} - 1\right). \tag{B7}$$

This expression describes the dotted hyperbolic arc in the bottom left corner of Fig. 4(a). The coordinates of the vertex (the right-most point) of the arc are readily obtainable from the condition $\partial\kappa/\partial h = 0$:

$$\kappa_v = \tfrac{1}{36}m(1-\sqrt{m})^2, \tag{B8}$$

$$h_v = \sqrt{m} - m. \tag{B9}$$

### 3. Coordinates of the critical points $C_1$ and $C_2$

Set $\beta = \pi/3$ or $2\pi/3$ into Eqs. (B1) and (B2) and solve them for $\alpha$ and $h$:

$$\alpha = \arcsin\left(\tfrac{1}{2}\sqrt{3}m\right), \tag{B10}$$

$$h = \sqrt{1 - \tfrac{3}{4}m^2} \pm \tfrac{1}{2}m. \tag{B11}$$

Equation (B11) describes the ordinates of the points $C_1$ and $C_2$. The abscissae are given by

$$\kappa = \tfrac{1}{48}m^2\left(1 - \tfrac{1}{2}m^2 \pm m\sqrt{1 - \tfrac{3}{4}m^2}\right). \tag{B12}$$

The proof of this expression is given for the upper sign, corresponding to $\beta = \pi/3 + \eta$, where $\eta$ is a small angle. (The proof for the lower sign is fully analogous; one only needs to replace $m$ throughout by $-m$.) Setting $\beta = \pi/3 + \eta$ into the equilibrium condition [Eq. (B1)], one solves it for $\alpha$ to terms linear in $\eta$:

$$\alpha = \arctan\left(\frac{\sqrt{3}m}{2h-m}\right) + \frac{2m(h-2m)}{(2h-m)^2 + 3m^2}\eta + \cdots. \tag{B13}$$

The expression is then used to eliminate $\alpha$ from the second equilibrium condition (B2). To terms linear in $\eta$, the result is

$$\frac{\sqrt{3}mh}{\sqrt{(2h-m)^2+3m^2}} - \frac{\sqrt{3}}{2}mh + \frac{2mh(2h-m)(h-2m)}{[(2h-m)^2+3m^2]^{3/2}}\eta - \frac{mh}{2}\eta + 36\kappa\eta = 0. \tag{B14}$$

This equation describes implicitly the dependence $h(\eta)$, which in conjunction with an expression for $\sigma(\eta)$ can be regarded as a parametric description of the magnetization curve $\sigma$ versus $h$. At the critical point, the following conditions must be fulfilled: $\partial h/\partial\eta = 0, \partial\sigma/\partial\eta \neq 0$. Now, the full derivative of the left-hand side of Eq. (B14) with respect to $\eta$ equals identically 0. The partial derivative, $\partial/\partial\eta = d/d\eta - (\partial h/\partial\eta)\partial/\partial h$, must, therefore, vanish at the critical point. Differentiating (B14) with respect to $\eta$ at constant $h$, we, thus, find

$$\kappa = \frac{1}{36}\left\{\frac{mh}{2} - \frac{2mh(2h-m)(h-2m)}{[(2h-m)^2+3m^2]^{3/2}}\right\}. \tag{B15}$$

The sought expression [Eq. (B12)] is obtained by substituting Eq. (B11) for $h$ into Eq. (B15).

#### 4. Coordinates of the infinitely remote points $A_1$ and $A_2$ on the right of Fig. 4(a)

These are given by Eq. (8):

$$h_{1,2} = \frac{\sqrt{3m^4 + 16(1-m^2)} \pm \sqrt{3}m}{4 - \frac{3}{4}m^2}. \tag{B16}$$

To derive this expression, one has to take into consideration that at $\kappa = \infty$, the angle $\beta$ can only take one of three values corresponding to three equivalent easy orientations of $\boldsymbol{M}_{\mathrm{Ho}}$. Accordingly, three distinct phases are possible.

Phase 1: $\beta_1 = 5\pi/6$. Setting this value into Eq. (B1), we find

$$\alpha_1 = \arctan\left(\frac{m}{2h + \sqrt{3}m}\right). \tag{B17}$$

Substituting $\alpha_1$ and $\beta_1$ for $\alpha$ and $\beta$ in Eq. (4) and omitting the infinite term in $\kappa$, we get the energy of phase 1:

$$\phi_1 = -\sqrt{\left(h + \tfrac{1}{2}\sqrt{3}m\right)^2 + \tfrac{1}{4}m^2} + \tfrac{1}{2}\sqrt{3}m. \tag{B18}$$

Phase 2: $\beta_2 = \pi/2$,

$$\alpha_2 = \arctan\left(\frac{m}{h}\right), \tag{B19}$$

$$\phi_2 = -\sqrt{m^2 + h^2}. \tag{B20}$$

Phase 3: $\beta_3 = \pi/6$,

$$\alpha_3 = \arctan\left(\frac{m}{2h - \sqrt{3}m}\right), \tag{B21}$$

$$\phi_3 = -\sqrt{\left(h - \tfrac{1}{2}\sqrt{3}m\right)^2 + \tfrac{1}{4}m^2} - \tfrac{1}{2}\sqrt{3}m. \tag{B22}$$

Equation (B16) is derived from the conditions of equality of the energies of phases, $\phi_1 = \phi_2$ (lower sign) and $\phi_2 = \phi_3$ (upper sign). Substituting $\alpha_1$ and $\beta_1$ or $\alpha_2$ and $\beta_2$ or $\alpha_3$ and $\beta_3$ for $\alpha$ and $\beta$ in Eq. (5), one obtains Eq. (7).

*skourski@hzdr.de


[1] J. M. D. Coey, *Magnetism and Magnetic Materials* (Cambridge University Press, Cambridge, 2009).

[2] At temperatures relevant to applications ($T \gtrsim 300$ K), the first anisotropy constant of a rare-earth magnet scales as $A_{20}H_{\mathrm{mol}}^2$ (Ref. 26).

[3] K. Clausen, Ph.D. thesis, Risø National Laboratory, 1981.

[4] K. Clausen and B. Lebech, J. Phys. C **15**, 5095 (1982).

[5] S. Sinnema, Ph.D. thesis, University of Amsterdam, 1988.

[6] S. Sinnema, J. J. M. Franse, R. J. Radwanski, A. Menovsky, and F. R. de Boer, J. Phys. F **17**, 233 (1987).

[7] P. C. M. Gubbens and K. H. J. Buschow, J. Phys. F **12**, 2715 (1982).

[8] X. F. Han, H. M. Jin, Y. Yan, and C. C. Sun, Phys. Status Solidi B **171**, K35 (1992).

[9] X. F. Han, H. M. Jin, T. S. Zhao, and C. C. Sun, J. Phys. Condens. Matter **5**, 8603 (1993).

[10] B. García-Landa, P. A. Algarabel, M. R. Ibarra, F. E. Kayzel, and J. J. M. Franse, Phys. Rev. B **55**, 8313 (1997).

[11] We use the notation of Ref. 10. Accordingly, the values of Refs. 3 and 4 had to be divided by the Stevens factor, $\gamma_J = -5/3864861$; the values of Refs. 8 and 9 were multiplied by $\sqrt{231}/16$; and the value of Ref. 10 was multiplied by $\langle r^6 \rangle = 5.379a_0^6$, taken from Ref. 27.

[12] M. S. S. Brooks, J. Phys. C **2**, 1016 (1969).

[13] $J^6$ in Eq. (18) of Ref. 3 should in fact be replaced by $J(J-\frac{1}{2})(J-1)(J-\frac{3}{2})(J-2)(J-\frac{5}{2})$ with $J = 8$.

[14] K. Clausen and O. Nielsen, J. Magn. Magn. Mater. **23**, 237 (1981).

[15] A. Sarkis and E. Callen, Phys. Rev. B **26**, 3870 (1982).

[16] M. D. Kuz'min, Y. Skourski, K. P. Skokov, and K.-H. Müller, Phys. Rev. B **75**, 184439 (2007).

[17] J. Wosnitza, A. Bianchi, J. Freudenberger, J. Haase, T. Herrmannsdoerfer, N. Kozlova, L. Schultz, Y. Skourski, S. Zherlitsyn, and S. Zvyagin, J. Magn. Magn. Mater. **310**, 2728 (2007).

[18] S. Zherlitsyn, A. Bianchi, T. Herrmannsdoerfer, F. Pobell, Y. Skourski, A. Sytcheva, S. Zvyagin, and J. Wosnitza, IEEE Trans. Appl. Supercond. **16**, 1660 (2006).

[19] G. P. Felcher and R. Kleb, Europhys. Lett. **36**, 455 (1996).

[20] I. S. Tereshina, S. A. Nikitin, J. Stepien-Damm, W. Suski, A. A. Salamova, and V. N. Verbetsky, J. Magn. Magn. Mater. **258**, 427 (2003).

[21] J. Franse, R. Radwański, and S. Sinnema, J. Phys. **49**, C8-505 (1988).

[22] S. V. Tyablikov, Fiz. Met. Metalloved. **3**, 3 (1956).

[23] A. E. Clark and E. Callen, J. Appl. Phys. **39**, 5972 (1968).

[24] M. D. Kuz'min, J. Magn. Magn. Mater. **322**, 1068 (2011).

[25] M. D. Kuz'min, Phys. Rev. B **79**, 212405 (2009).

[26] M. D. Kuz'min, Phys. Rev. B **51**, 8904 (1995).

[27] A. J. Freeman and J. P. Desclaux, J. Magn. Magn. Mater. **12**, 11 (1979).